# Two-hydrogenic vertically stacked $Ga_{1-x}Al_xAs$ nanoscale rings: simultaneous effects of hydrostatic pressure, aluminum concentration, magnetic field and temperature on the quantum levels

J. D. Castrillón[a,*], D. A. J. Gómez-Ramírez[b], I. E. Rivera[c], Y. A. Suaza[a], J. H. Marín[a], M. R. Fulla[a,c]

[a] *Escuela de Física, Universidad Nacional de Colombia, A. A. 3840, Medellín, Colombia*
[b] *Vienna University of Technology, Wiedner Hauptstrasse 8-10, 1040, Vienna, Austria*
[c] *Institución Universitaria Pascual Bravo, A. A. 6564, Medellín, Colombia*

**Abstract**

The low-lying energy levels of two on-axis shallow donor impurities releasing two electrons in two vertically stacked $Ga_{1-x}Al_xAs$ nanorings are calculated. The analysis has been focused on the effects of the hydrostatic pressure (P), aluminum concentration ($Al_x$) and temperature (T) in the quantum energy levels ordering. It was obtained that in the ranges $0-15$ *kbar* of hydrostatic pressure, $4-400$ $K$ of temperature, and $0-0.4$ of aluminum concentration, the variable that generates the greatest energy variation is the aluminum concentration, and that the aluminum concentration and hydrostatic pressure tends to favor the molecular stability while the temperature has a contrary effect. The two-particle Wigner crystallization is affected by the (P,$Al_x$,T) factors and the transition points may vary from state to state. The ground state energy parameters of the artificial molecule such as the equilibrium length and dissociation energy can be substantially modified through the inter-ring distance and the rings radii, respectively. The effects of the (P,$Al_x$,T) factors affects the molecular ground state energy in the order of $3-5\%$.

*Keywords:* Artificial two-hydrogen molecule, Quantum rings, Ring-like

*Corresponding author
*Email address:* marlonfulla@yahoo.com (M. R. Fulla)

nanostructure, Wigner crystallization

## 1. Introduction

Recent significant advancements in semiconductor nanostructure engineering have highly improved the growth of single vertically stacked pairs of quantum dots (QDs) with modifiable vertical dot-dot spacing [1, 2]. In lattice-mismatched heteroepitaxy, vertical self-alignment of QDs is obtained as a consequence of a strain field into the spacer layer by the first QD layer favoring the growth of a second QD above the first one [2, 3]. Morphological and structural analyses of vertical coupled quantum dots (VCQDs) are being currently carried out thorough multibeam bright field imagining, and surface morphology characterization, with atomic force microscopy [4]. With the purpose of studying their optical features; spectroscopy (micro-photoluminescence and photoluminescence excitation), and time-resolved techniques [2] are being used. Very recently, Elborg and co-workers [5] have sucessfully grown vertically aligned GaAs quantum ring/dot structures by a multiple droplet epitaxy technique. They show that the geometry of the rings and dots, and the GaAlAs spacer layer, can be controlled in separated growth steps. In parallel, Heyn [6] fabricated self-aligned vertically stacked GaAs quantum dot molecules by filling of self-assembled nanoholes in a GaAlAs matrix. In this work was shown the excitonic features exhibited by the quantum dot molecules by studying their optical emission. These experimental findings have revealed the great potential offered by VCQDs for fabricating complex quantum molecules oriented to the development of quantum information technologies [3, 7]. One huge value concerning these quantum-based computational devices could be related to alternative ways of constructing more efficient computational paradigms and tools aiming to solve complex problems in a human-style such as the denominated artificial (mathematical) agents [8, 9, 10]. Consequently, in order to delve deeper into the understanding of the physical phenomenon underlying, several theoretical works on few-particle systems confined in VCQDs have been addressed [11, 12, 13, 14, 15, 16]. Manjarres [11]

calculated some low-lying states of a double-donor complex confined in vertically coupled quantum lenses, threaded by a uniform magnetic field, as a function of the interdot distance and the magnetic field strength. The results show that the complex evolves from a ordered system (in which the charge carriers behave as a rigid rotator) to a disordered one (similar to a gas-like system) by decreasing the lenses size. In [12] the authors calculated the quantum states and recombination probabilities for excitons, and negative and positively charged trions in VCQDs under the presence of an electric field. It was shown that the exciton and trions energies as a function of the electric field, exhibit crossing and anticrossing points which can be interpretated as a proof of the fact that the exciton or trion can be tuned into resonance states by the electric field applied. Stavrou [13] employed the strain dependent $\vec{k} \cdot \vec{p}$ theory to analyze the relationship between the circular light polarization and the size asymmetry of self-assembled VCQDs with ellipsoidal shape. The results show that the circular light polarization takes large values if enlongated QDs, small dot-dot spacings and large volumes ratios are considered. Computational calculations of magnetization and differential magnetic susceptibility for single-electron semiconductor vertical coupled quantum rings (VCQRs) have been addressed by Li [14], showing that the magnetic field threading through the nanostructure yields to non-periodical jumps of the magnetization which are dependent on the radii of the rings and the ring-ring spacing. Additional studies related to the effect of the quantum dot morphology on the binding energy of a neutral donor confined in two VCQDs has been perfomed [15, 16]. The studies concluded that the neutral donor binding energy it is strongly dependent on the quantum dot size and shape.

Undoubtedly, these experimental and theoretical reports evince that semiconductor VCQDs are a promising scenario to develop innovating quantum physics. Since the two-electron VCQRs in hard confinement have been previously addressed in [17], performing one additional step, would motivate to study three-dimensional structures compound by VCQRs confining other few-particle systems such as the artificial $H^-$ and $Li^+$ ions, or artificial $He$ atoms, in order to explore the structure-to-structure interaction and geometrical effects on the

energy spectrum of such artificial nanosystems. Since there are not too many reports in the literature analyzing double-donor systems confined in VCQRs, also called two-hydrogenic artificial complexes, in the present work, we have undertaken a theoretical study to calculate the eigenenergies and eigenstates of two electrons spatially separated and forced to move in two $Ga_{1-x}Al_xAs$ VCQRs and bounded to two on axis-fixed shallow donors. The full system is under hydrostatic pressure and external magnetic field probes. We have analyzed the effects on the quantum levels due to the magnetic field, the aluminum concentration, the temperature and the hydrostatic pressure, being this last effect interesting since the low-temperature photoluminescence spectra measurements in semiconductor QDs under hydrostatic pressure have shown that this external probe modifies significantly the carrier energy structure [18].

## 2. Theoretical Framework

The few-particle system analyzed in the present work is shown in Fig. (1). Two electrons released by two on-axis shallow donor impurities are trapped inside of two parallel $Ga_{1-x}Al_xAs$ toroidal nanorings with radii $R_1$ (lower toroid) and $R_2$ (upper toroid), both with identical cross-section areas equal to $\pi {R_t}^2$.

The two-toroid system is in presence of a growth-direction magnetic field $\vec{B}$ (z-direction), being $d$ the interplanar separation between the toroids. In order to ease the analysis and focus the attention on the structure-structure interaction, it was consider an insulating material matrix with the same elastic properties and static permittivity of the QRs' material. The positions of the impurities in the insulating matrix are defined by $\vec{\xi_1} = (0, 0, -\xi_1)$ and $\vec{\xi_2} = (0, 0, \xi_2)$. Additionally, an applied hydrostatic pressure field $P$ is applied on the overall system. Since the changes of hydrostatic pressure, aluminum concentration and temperature have an important incidence on the electron's effective mass $m^*(P, x, T)$, the static permittivity $\epsilon(P, T)$, and particularly the hydrostatic pressure on the structural dimensions of the system [19, 20, 21], we have defined a set of effective units at standard conditions ($P = 0$, $x = 0$, and $T = 4\ K$)

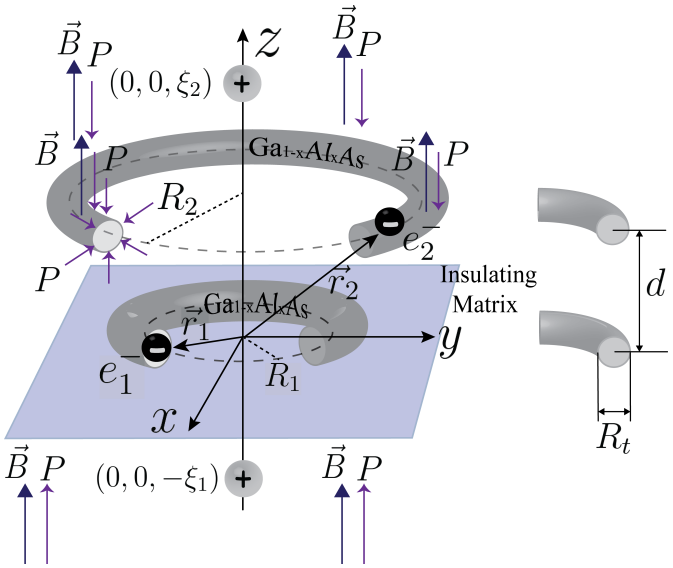


Figure 1: Schematic model of the two-hydrogenic $Ga_{1-x}Al_xAs$ VCQRs under the presence of a magnetic field and hydrostatic pressure.

to scale the $P$, $x$, $T$-dependent system Hamiltonian, these are the effective Bohr radius $a_0^* = \frac{\hbar^2(4\pi\epsilon(0,4))}{m^*(0,0,4)e^2}$, the effective Rydberg $Ry^* = \frac{m^*(0,0,4)e^4}{2\hbar^2(4\pi\epsilon(0,4))^2}$, and $\gamma = \frac{\hbar eB}{2m^*(0,0,4)cRy^*}$, as units of length, energy, and dimensionless magnetic field strength, respectively. Within the framework of the effective-mass approximation, the dimensionless system Hamiltonian in cylindrical coordinates can be written as:

$$\hat{H} = \sum_{j=1}^{2} \hat{H}_0(\vec{r}_j) + \frac{2}{\sigma(P,T)|\vec{r}_2 - \vec{r}_1|} + \frac{2}{\sigma(P,T)|\vec{\xi}_2 - \vec{\xi}_1|} \tag{1a}$$

$$\hat{H}_0(\vec{r}_j) = -[\frac{1}{\rho_j}\frac{\partial}{\partial\rho_j}\Big(\frac{\rho_j}{\mu(P,x,T)}\Big)\frac{\partial}{\partial\rho_j} + \frac{1}{\mu(P,x,T)\rho_j^2}\frac{\partial^2}{\partial\varphi_j^2} + \frac{\partial}{\partial z_j}\Big(\frac{1}{\mu(P,x,T)}\Big)\frac{\partial}{\partial z_j}] - \frac{i\gamma}{\mu(P,x,T)}\frac{\partial}{\partial\varphi_j} + \frac{\gamma^2\rho_j^2}{4\mu(P,x,T)} + \sum_{k=1}^{2}\frac{2}{\sigma(P,T)|\vec{r}_j - \vec{\xi}_k|} + V_j(\vec{r}_j) \tag{1b}$$

where the dimensionless scalar functions $\sigma(P,t) = \epsilon(P,T)/\epsilon(0,4)$ and $\mu(P,x,T) =$

$m^*(P,x,T)/m^*(0,0,4)$ describe the static permittivity and electron's effective mass dependency on the $(P,x,T)$ values, repectively. The first term in Eq. (1a) corresponds to the one-electron hamiltonian (see Eq. (1b)) containing the kinetic energy operator (first term between brackets), the magnetic couplings (second and third terms), the electron-impurities interactions (fourth term) and the quantum confinement $V_j(\vec{r}_j)$ due to the energy gap difference between the materials (assumed to be zero inside the toroids walls and infinity in the insulating matrix). The second and third terms in Eq. (1a) are related to the electron-electron and impurity-impurity Coulomb interactions, respectively. According to Refs. [19, 20, 21] the $P$, $x$, $T$-dependent electron's effective mass $m^*(P,x,T)$ in the $Ga_{1-x}Al_xAs$ QRs can be written as follows:

$$m^*(P,x,T) = m_0\Big[1+\delta(x)+\frac{\Pi^2(x)}{3}\Big(\frac{2}{E_g^\Gamma(P,x,T)}+\frac{1}{E_g^\Gamma(P,x,T)+\Delta_0(x)}\Big)\Big]^{-1} \tag{2a}$$

$$E_g^\Gamma(P,x,T) = a_\Gamma + b_\Gamma x + c_\Gamma x^2 + \alpha_\Gamma P - \beta_\Gamma T^2(\gamma_\Gamma+T)^{-1} \tag{2b}$$

being $m_0$ the free electron mass, $\Pi^2(x)$ the square of the interband matrix element describing the coupling between the $s$ states of the conduction band with the hybrid $sp$-valence states, $\Delta_0(x)$ the split-off valence gap, and $E_g^\Gamma$ the energy gap. The remote-band effects are considered into the $\delta(x)$ term. The explicit form of all the previous quantities and the fitting constants were extracted from Refs. [19, 20, 21]. The static permittivity dependent on the hydrostatic pressure and temperature $\epsilon(P,t)$ is given by Ref. [20]:

$$\epsilon(P,T) = \kappa_1(T)e^{\kappa_2(T)T-\kappa_3(T)P} \tag{3}$$

where the $\kappa_1(T)$, $\kappa_2(T)$, and $\kappa_3(T)$ fitting parameters depend on the current temperature of the system [20]. The effect of the hydrostatic pressure field on the two-toroid structure is reflected in the dependence of the geometrical parameters (toroids cross-section areas $\pi {R_t}^2$ and the toroids radii $R_1$ and $R_2$), the interplanar toroid-toroid separation $d$, and the impurity positions ($\xi_1$ and

$\xi_2$) on the hydrostatic pressure strength $P$. We have assumed those functional dependencies from Ref. [21]:

$$\frac{\xi_j(P)}{\xi_j(0)} = [1 - (S_{11} + 2S_{12}P)] \tag{4a}$$

$$\frac{R_j(P)}{R_j(0)} = [1 - 2(S_{11} + 2S_{12}P)]^{1/2} \tag{4b}$$

where $S_{11}$ and $S_{12}$ are the compliance constants. The Eqs.(4a-4b) describe the axial and radial dimensional reduction percentage due to the applied hydrostatic pressure.

The Hamiltonian (1a) it is not exactly solvable, but bearing in mind the experimental fact that self-assembled quantum rings have a small height-to-base aspect ratio [22], it is possible to solve it by using the well-known adiabatic procedure [23, 24]. The method begins by finding from Eq. (1a) the numerical two-electron ground-state wave function $f_{\varphi_1}(\vec{r}_1)f_{\varphi_2}(\vec{r}_2)$ and its corresponding energy $E_{adiab}(\varphi_1, \varphi_2)$ for fixed values of $\varphi_1$, $\varphi_2$. Reintroducing the adiabatic energy $E_{adiab}$ leads to the following $\varphi_1$,$\varphi_2$-dependent eigenvalue problem:

$$\begin{aligned}\hat{H}_a = \sum_{j=1}^{2}[-\frac{1}{\mu(x,P,T)}\frac{\partial^2}{\partial\varphi_j^2} - \frac{i\gamma}{\mu(x,P,T)}\frac{\partial}{\partial\varphi_j} + \frac{\gamma^2 A_j(\varphi_j)}{4\mu(x,P,T)}] + E_{adiab} \\ + V_{ee}(\varphi_2 - \varphi_1) + \sum_{j=1}^{2}\sum_{k=1}^{2} V_{e_j,i_k} + \frac{2}{\sigma(P,T)|\vec{\xi}_2 - \vec{\xi}_1|}\end{aligned} \tag{5a}$$

$$A_j(\varphi_j) = \int_{CS} |\rho_j \ f_{\varphi_j}(\vec{r}_j)|^2 dS_j \tag{5b}$$

$$V_{ee}(\varphi_2 - \varphi_1) = \frac{2}{\sigma(P,T)}\int_{CS} \frac{|f_{\varphi_1}(\vec{r_1})f_{\varphi_2}(\vec{r_2})|^2}{|\vec{r}_2 - \vec{r}_1|} dS_1 dS_2 \tag{5c}$$

$$V_{e_j,i_k} = \frac{-2}{\sigma(P,T)}\int_{CS} \frac{|f_{\varphi_1}(\vec{r_1})f_{\varphi_2}(\vec{r_2})|^2}{|\vec{r}_j - \vec{\xi}_k|} dS_1 dS_2 \tag{5d}$$

The (5c) and (5d) terms represent the electron-electron and electron-impurities mean-potentials integrated over the toroids cross-section (CS) and dependent

only on $\varphi_1$ and $\varphi_2$ (the slow rotational motion has been decoupled from the fast transverse motion). Futhermore, the two-electron dynamics can be described more properly by using the center-of-mass $\Theta = \frac{R_1^2\varphi_1 + R_2^2\varphi_2}{R_1^2 + R_2^2}$ and relative $\varphi = \varphi_2 - \varphi_1$ coordinates, since the adiabatic Hamiltonian can be rewritten as $\hat{H}_a = \hat{H}_\Theta + \hat{H}_\Phi$, where the center-of-mass and relative operators establish the eigenvalue equations, $\hat{H}_\Theta \Psi_M(\Theta) = E_\Theta(M)\Psi_M(\Theta)$ and $\hat{H}_\Phi \Phi_{m,s}(\varphi) = E_\Phi(m,s)\Phi_{m,s}(\varphi)$, respectively. The first equation with Hamiltonian $\hat{H}_\Theta$ can be solved exactly, whilst the another one was solved numerically by using a diagonalization matrix scheme [25] with periodic boundary conditions in the region $[-2\pi, 2\pi]$ defined by the expression $\Phi_{m,s}(\varphi) = (-1)^M \Phi_{m,s}(\varphi \pm 2\pi)$. The quantum numbers $M = 0, \pm 1, \pm 2, ...$ and $m = 0, \pm 1, \pm 2, ...$ denote the center-of-mass angular momentum and the two-electron relative angular momentum, respectively. On the other hand, $s = +$ denotes even solutions or singlet states, whilst $s = -$ denotes odd solutions or triplet states.

## 3. Results and Discussion

### *3.1. Results validation*

With the aim of establishing the quality of our numerical procedure, we have calculated the eigenergies from Eq. (1a) multiplied by $R_1^2$ (also known as renormalized eigenergies) in order to compare them with the results obtained by Zhu and co-workers [26], who calculated exactly the eigenstates and renormalized eigenergies of two electrons hardly confined in a GaAs one-dimensional quantum ring.

In Table 1, is displayed the renormalized eigenergies of a two-hydrogenic VCQR system at zero magnetic field in the following limit conditions, equal mean radii ($R_1 = R_2$), cross-section radii equal to 0.001 $a_0^*$, ring-ring separation of 0.002 $a_0^*$, and with the impurities located far away from the origin at the positions $\xi_1 = \xi_2 = 10000\ a_0^*$. In such limit conditions, our two-hydrogenic VCQR behaves similarly to the two-electron system hardly confined studied in Ref. [26]. The results are organized as follows, in the first column is placed the

Table 1: Comparison between the set of renormalized eigenenergies of a two-hydrogenic VC-QRs system in limit conditions (present work) and those obtained by Ref. [26].

| | State | (0,0,0) | | | (1,1,1) | | | (2,2,0) | | |
|---|---|---|---|---|---|---|---|---|---|---|
| | Radius | 1 $a_0^*$ | 4 $a_0^*$ | 20 $a_0^*$ | 1 $a_0^*$ | 4 $a_0^*$ | 20 $a_0^*$ | 1 $a_0^*$ | 4 $a_0^*$ | 20 $a_0^*$ |
| P | 30 $kbar$ | 1.74334 | 5.42441 | 23.83662 | 2.16474 | 5.84650 | 24.25877 | 7.51071 | 12.76754 | 35.75066 |
| | 15 $kbar$ | 1.73330 | 5.29618 | 23.08026 | 2.18992 | 5.75351 | 23.53769 | 7.90329 | 13.03544 | 35.46388 |
| | 10 $kbar$ | 1.73126 | 5.24653 | 22.58104 | 2.20116 | 5.71712 | 23.05175 | 8.05366 | 13.13630 | 35.14318 |
| | 1 $kbar$ | 1.73221 | 5.19075 | 22.42068 | 2.22828 | 5.68748 | 22.91757 | 8.35622 | 13.37911 | 35.33673 |
| | 0.1 $kbar$ | 1.73182 | 5.17439 | 22.12777 | 2.23070 | 5.67392 | 22.62745 | 8.38811 | 13.39476 | 35.08173 |
| | Ref. [26] | 1.73248 | 5.18378 | 22.37530 | 2.23167 | 5.68362 | 22.87530 | 8.39238 | 13.40774 | 35.33351 |
| T | 400 $K$ | 1.74115 | 5.06550 | 21.58679 | 2.29911 | 5.62385 | 22.14544 | 9.07863 | 13.95939 | 35.32773 |
| | 200 $K$ | 1.73245 | 5.13070 | 22.04273 | 2.25230 | 5.65112 | 22.56336 | 8.62941 | 13.58712 | 35.27014 |
| | 40 $K$ | 1.72982 | 5.17049 | 22.30745 | 2.23032 | 5.67163 | 22.80875 | 8.40337 | 13.40530 | 35.27316 |
| | 10 $K$ | 1.73189 | 5.18137 | 22.36362 | 2.23115 | 5.68128 | 22.8637 | 8.39238 | 13.40533 | 35.32069 |
| | 6 $K$ | 1.73228 | 5.18297 | 22.37139 | 2.23148 | 5.68282 | 22.87141 | 8.39229 | 13.40683 | 35.32909 |
| | Ref. [26] | 1.73248 | 5.18378 | 22.37530 | 2.23167 | 5.68362 | 22.87530 | 8.39238 | 13.40774 | 35.33351 |
| $Al_x$ | 0.4 | 1.55557 | 4.94106 | 21.92085 | 1.89260 | 5.27862 | 22.25844 | 6.24830 | 11.02882 | 31.96288 |
| | 0.3 | 1.58535 | 4.98330 | 22.00128 | 1.94903 | 5.34757 | 22.36560 | 6.60319 | 11.42982 | 32.54519 |
| | 0.1 | 1.67288 | 5.10406 | 22.22812 | 2.11650 | 5.54837 | 22.67252 | 7.66146 | 12.60714 | 34.22062 |
| | 0.01 | 1.72536 | 5.16511 | 22.10754 | 2.21846 | 5.65887 | 22.60145 | 8.31185 | 13.31055 | 34.96138 |
| | Ref. [26] | 1.73248 | 5.18378 | 22.37530 | 2.23167 | 5.68362 | 22.87530 | 8.39238 | 13.40774 | 35.33351 |

different values of hydrostatic pressure, temperature and aluminum concentration used to calculate the corresponding renormalized energies for three different radii 1 $a_0^*$, 4 $a_0^*$, and 20 $a_0^*$ (labeled in the second row of the table). This calculation was performed for the ground state $(0, 0, 0)$ (columns two to four) and the excited states $(1, 1, 1)$ (columns five to seven) and $(2, 2, 0)$ (columns eight to ten). For instance, by decreasing the hydrostatic pressure strength from 30 $kbar$ to 0.1 $kbar$, one can see that our renormalized eigenenergies in the three quantum states independently of the radius value (e.g. from the smaller to the bigger one) tend to the renormalized energies calculated by Ref. [26] (eighth shaded row).

Additionally, as the temperature and the aluminum concentration decreases from 400 $K$ to 6 $K$, and 0.4 to 0.01, respectively, the renormalized energies also tend to the values calculated by Zhu [26] (shaded rows). This correct tendency was expected since the effective atomic units used by Zhu correspond to GaAs materials ($Al_x = 0$) at 4 $K$, and at zero hydrostatic pressure field. This fact can be interpreted as an indirect quality proof of our numerical procedure obtained with the two-hydrogenic VCQRs model giving an account of the results obtained for similar systems which could be conceived as particular cases of the model proposed in the present work. It is necessary to emphasize that the convergence to the Ref. [26] values in some cases is strictly non-monotonous, for instance in state $(2, 2, 0)$ and radius 20 $a_0^*$, the corresponding renormalized eigenenergies to the hydrostatic pressure values of 10, 1 and 0.1 $kbar$ are 35.14318, 35.33673, and 35.08173 $Ry^* {a_0^*}^2$. This fact obeys to the complex interplay among the terms of the system Hamiltonian in Eqs. (1a) and (1b) due to the hydrostatic pressure, temperature, and $Al_x$ concentration. The ($P$,$x$,$T$) interplay in association with the two-toroid geometric variations and external fields is subject of study in the subsequent sections.

### *3.2. Effect of the hydrostatic pressure*

In order to discuss and visualize adequately our numerical results for the states $(M, m, s)$, throughout this contribution, we will analyze the ground state $(0, 0, 0)$ and the excited states $(\pm1, 1, 0)$, $(\pm2, 2, 0)$, $(\pm1, 3, 0)$. This set of states will give us a general idea of the system's behavior and will make clear the interpretation avoiding the multiple curves overcrossing. In Fig. (2) it is displayed the renormalized energy for some low-lying levels as a function of the lower ring radius $R_1$ for different hydrostatic pressure values 0, 15 and 30 $kbar$. The aluminum concentration $\mathrm{Al}_x$ and the magnetic field strength are fixed to zero, the ring-ring separation is 1 $a_0^*$, the on-axis donor-donor distance is 2 $a_0^*$, and the temperature of the sample is set to 4 $K$.

At a first glance, the renormalized energy values for the shown low-lying levels can be reduced by increasing the hydrostatic pressure field strength within

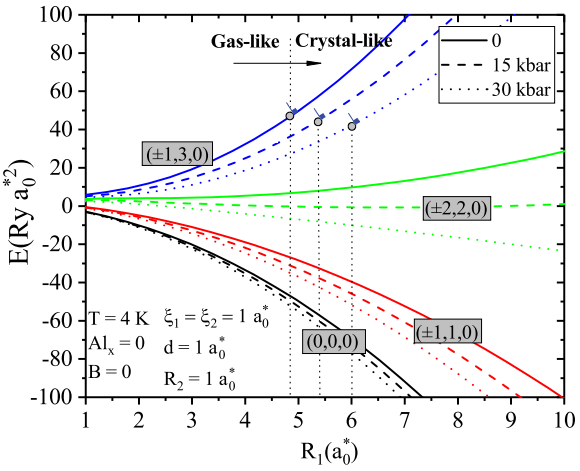


Figure 2: Renormalized energy as a function of $R_1$ for different values of the hydrostatic pressure. The arrow depicts that for large values of $R_1$, the two-hydrogenic VCQRs evolves from a gas-like to a crystal-like system.

the range $0 - 30$ *kbar*, being this an indicator that in general the hydrostatic pressure increases the two-hydrogenic complex stability. This behavior is linked mainly to the direct relation between the effective mass and the hydrostatic pressure in Eq.(2a), since for greater values of the hydrostatic pressure, the electron mobility decreases as a consequence of the increment of its effective mass. In particular, the levels $(0, 0, 0)$ and $(\pm 1, 1, 0)$ are of special interest since they are bounded states due to the negative energy values, which is desirable in diverse technological applications. Also, it can be seen that the ground state is the least sensitive to hydrostatic pressure changes.

In addition, it can be seen that for $R_1$ values smaller than 6 $a_0^*$ the eigenenergies undergoes drastic changes in the slope curve, and on the contrary, for greater values than 6 $a_0^*$, the slopes tend to a quasi-constant behavior indicating a transition from a disordered system similar to a gas-like configuration to a ordered one with the features of a rigid rotor. This fact is easily to explain thorough a one-dimensional models [17] which predicts that for large $R_1$ val-

ues the renormalized kinectic energy tend to be independent on the ring radii and the renormalized potential energy tends to be proportional to $R_1$. A similar phenomenon has been seen before for the case of two electrons in quantum rings [17] and lenses [11], and it can be interpreted as a two-particle Wigner crystallization.

It is necessary to emphasize that the $R_1$ value in which the transition from a gas-like to a crystal-like system is given, may vary depending on the state and the external fields applied. For instance, in Fig.2, it was drawn perpendicularity symbols on the curves of the state $(\pm 1, 3, 0)$ at the points $R_1 = 4.85,\ 5.37$ and $6\ a_0^*$ corresponding to the hydrostatic pressure values of $0, 15$ and $30\ kbar$, respectively. The perpendicularity symbols try to evince a tendency of the curves slope to behave quasi-constantly for greater values than those in which the perperdicularity symbols are drawn, so in this sense, the previously mentioned values of $R_1$ can be considered as gas-to-crystal transition points for each corresponding hydrostatic pressure considered. In other words, for this particular state, it can be infered that if the hydrostatic pressure is increased, larger values of $R_1$ are required in order to obtain the two-particle Wigner crystallization. The transition points for the other states at the different hydrostatic pressure conditions can be easily read by examining the quasi-constant behavior of the curves slopes.

### *3.3. Effect of the sample temperature*

In Fig. 3 is displayed the renormalized energy as a function of $R_1$ for values of the sample temperature equal to 4, $200K$ and, $400K$. Within the range of 1 and 10 $a_0^*$ for $R_1$, the energy levels of the analyzed states raise as the temperature of the sample is increased, being this effect more noticeable in excited states and in configurations with larger $R_1$ radius. This response was expected and linked mainly to the inverse variation between the effective mass and the temperature in Eq.(2a), since for greater values of the temperature, the electron mobility increases as a consequence of the reduction of its effective mass. For instance, the renormalized energy variations for a symmetric two-

hydrogenic VCQRs configuration with equal radii $R_1 = R_2 = 1\ a_0^*$, are of the order of units of Rydberg for excited states and tenths of Rydberg for the ground state case.

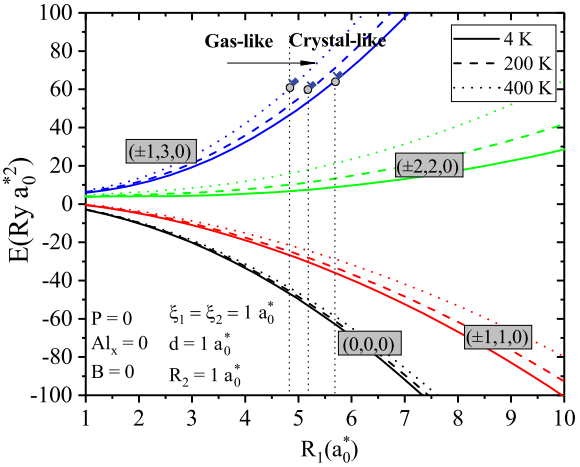


Figure 3: Renormalized energy as a function of $R_1$ for different values of the sample temperature.

On the other hand, the two-particle Wigner crystallization transition points for the state $(\pm 1, 3, 0)$ are $R_1 = 4.86,\ 5.15$ and $5.69\ a_0^*$ (see the perperdicularity symbols on the curves for the corresponding values of $T = 400,\ 200$, and $4\ K$, respectively). Consequently, for this particular state it can be inferred that the greater the temperature is the smaller the values of the transition points $R_1$ are.

### *3.4. Effect of the Aluminum concentration*

In Fig. 4 is plotted the renormalized energy as a function of $R_1$ for Aluminum concentration values of 0, 0.3, and, 0.4. It can be appreciated a general behavior of the analyzed energy levels which decreases as the Aluminum concentration increases within the range of $R_1$ from 1 to 10 $a_0^*$. The renormalized energy changes are small in the ground state in comparison with those for excited states, which is in accordance with the discussion in the previous sections. Nevertheless,

by varying the aluminum concentration from 0 to 0.4, one can obtain more drastic changes in the renormalized energy spectrum (specially in excited sates) in comparison with those obtained by varying the hydrostatic pressure from 0 to 15 *kbar* (see Fig. 2) or the temperature from 4 $K$ to 400 $K$ (see Fig. 3). Consequently, it is possible to state that the predominant variable among the sample temperature, the hydrostatic pressure and the aluminum concentration in a two-hydrogenic VCQRs system is the aluminum concentration, since can affect drastically the electron mobility due to the significant increase in effective mass.

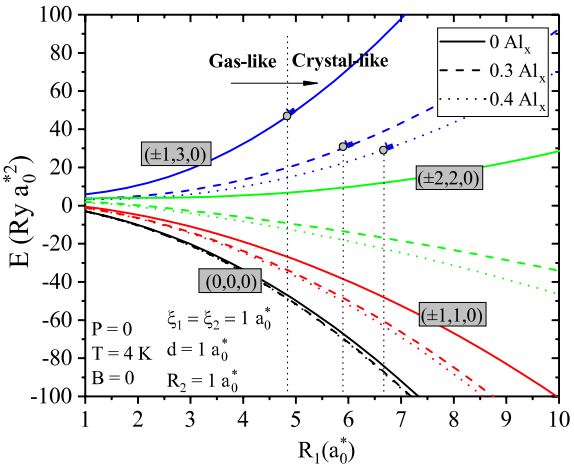


Figure 4: Renormalized energy as a function of $R_1$ for different values of the aluminum concentration.

The transition points for the state $(\pm 1, 3, 0)$ in which the Wigner crystallization takes place on the curves with $Al_x = 0,\ 0.3$, and 0.4 are respectively $R_1 = 4.84,\ 5.9$, and $6.66\ a_0^*$. Similarly such as the case with hydrostatic pressure, here the greater the values of $Al_x$ are the greater the values of $R_1$ (transition points) are.

All the results discussed in the previous subsections clearly show that the hydrostatic pressure, the sample temperature and aluminum concentration have a strong influence on the two-hydrogenic VCQRs level ordering and on its geom-

etry. Nevertheless, the presence of a magnetic field and the inter-ring distance affects significantly the energy level ordering as it is shown in the following subsection.

### 4. Effects on the magnetic field and inter-ring distance

In Fig. 5 is displayed the total energy as a function of the inter-ring distance for a two-hydrogenic VCQRs system with equal radii (1 $a_0^*$) and with their donors placed at $\xi_1 = \xi_2 = 1\ a_0^*$ and for the three different values of renormalized magnetic field $\gamma = 0$ (solid lines), 0.1 (dashed lines), and 0.5 (dotted lines). In the left (right) panel are displayed the energies of the four states previously analyzed with $M > 0$ ($M < 0$). It can be seen a general behavior of the energy levels when the rings begin to be separated starting from 0.01 $a_0^*$ to 2 $a_0^*$. As expected the all energy levels become to decrease as a consequence of the electron-electron term weakening but a minimum is reached at $d = 1\ a_0^*$ just when one of the rings is directly in front of one of the donors which provides the maximum stability that is feasible to obtain with this configuration since maximizes the approaching among positive and negative charged carriers.

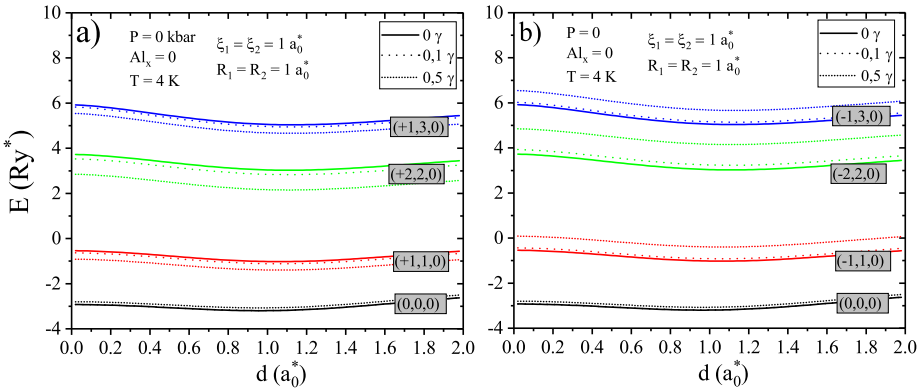


Figure 5: Renormalized energy as a function of the inter-ring distance for different values of the magnetic field strength.

In addition in Fig.5 can be seen two contrary effects by increasing the renor-

malized magnetic field intensity. In the left (right) panel the energy levels decrease (increase) as the the $\gamma$ parameter is increased. This is a consequence of the paramagnetic term of the system Hamiltonian (5a) whose contribution to the total energy is of the form $-M\gamma$, making the energy smaller (greater) when values of the quantum angular momentum $M > 0$ ($M < 0$) are taken.

## 5. Molecular features of the two-hydrogenic nanorings

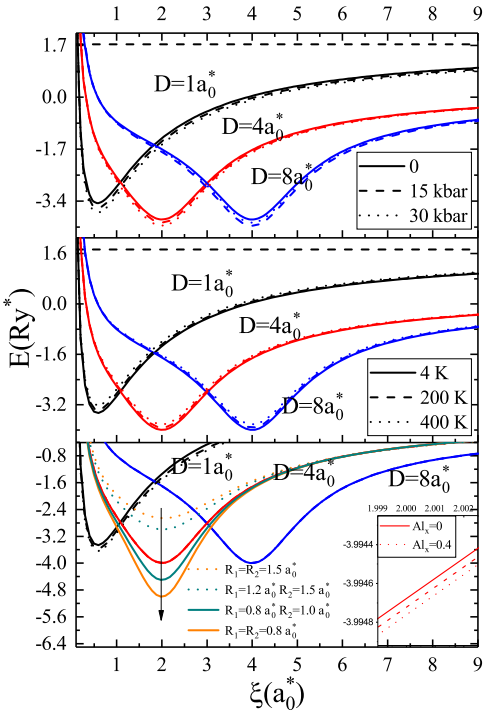


Figure 6: Total energy as a function of the donor-donor distance for different ring-ring distances. In all panels the black, red and blue curves correspond to a ring- ring distance equal to $d$ = 1,4, and 8 $a_0^*$ and the rings have equal radii $R_1 = R_2 = 1$ $a_0^*$.

In Fig. 6 is displayed the ground state energy of the two-hydrogenic VCQRs system as a function of the donor-donor separation. In all panelsthe total energy

is displayed for three different values of inter-ring distance $d = 1\ a_0^*$ (black lines), $4\ a_0^*$ (red lines), and $8\ a_0^*$ (blue lines). In the upper panel we vary the hydrostatic pressure thorough the values $P = 0$ (solid lines), 15 (dashed lines), and 30 $kbar$ (dashed lines). In the middle panel the temperature is varied thorough the values $T = 4$ (solid lines), 200 (dashed lines), and 400 $K$ (dashed lines). In the lower panel, the aluminum concentration is varied thorough the values $Al_x = 0$ (solid lines), 0.2 (dashed lines), and 0.4 (dashed lines).

At first glance, it is evident the close similarity with the curves of the molecular energy of a natural two-hydrogen molecule $H^2$. But unlike the natural molecule case, in our system by varying the inter-ring distance, it is possible to modify substantially the equilibrium length of the artificial molecule. In addition, by varying the hydrostatic pressure, temperature and aluminum concentration, it is possible to vary slightly the dissociation energy, making the molecule more stable if the hidrostatic pressure or the aluminum concentration is increased, and in the contrary, making the molecule more unstable if the temperature is increased. It is important to notice that the variations with the aluminum concentration are very small, even not noticeable in the curves with $d = 4$ and $8\ a_0^*$. For this reason, an inset in the lower panel was added to show the variations of the order of tenths of thousandths with the $Al_x$.

Finally, there is a mechanism to modify more significantly the dissociation energy thorough geometrical changes such as the ring radii. the olive and orange curves were plotted for the inter-ring distance $d = 4\ a_0^*$. The orange curve (small radii) is related to an more stable molecule due to the greater approaching between the electrons to the on-axis donors, while the dotted orange curve (large radii) defines a more unstable molecule by the opposite reason in the first case.

## 6. Conclusions

The simultaneous effects of hydrostatic pressure, aluminum concentration and sample temperature on the quantum levels of a two-hydrogenic VCQRs

under the presence of a uniform magnetic field were analyzed. The proposed adiabatic-based model is versatile enough to be compared with systems with different dimensionality such as two-electron one-dimensional quantum rings. The impact of this fact lies in the possibility of establishing successful qualitative comparisons with non-trivial systems with exact solutions. It was shown that the analyzed two-hydrogenic VCQRs energy levels are declined by an increase in hydrostatic pressure or aluminum concentration in the range of $0-15$ *kbar* and $0-0.4$, respectively, while the energy levels are raised by an increase of the temperature sample in the range of $4-400K$. By comparing these three effects one can conclude that the most drastic changes can be obtained by varying the aluminum concentration within the range $0-0.4$. These physical variables in association with the two-hydrogenic VCQRs geometry can be manipulated with the purposes of modifying the level ordering affecting the dynamics of the charge carriers (favoring or disfavoring crystallization Wigner-like process) for technological purposes.

## 7. Acknowledgements

This work was financially supported by the Universidad Nacional de Colombia through the *Convocatoria nacional de proyectos para el fortalecimiento de la investigación de la Universidad Nacional de Colombia 2016-2018* with grant number Código QUIPU: 201010017819 (research project entitled: *Estudio de las propiedades opto-electrónicas de los sistemas de una y dos partículas confinados en anillos y cintas cuánticas con deformaciones estructurales* (Código Hermes: 35461)) and by Institución Universitaria Pascual Bravo thorough the research project entitled: *Cálculo de propiedades electrónicas de nano-estructuras semiconductoras cuasi-bidimensionales con deformaciones estructurales por el método de elementos finitos* (Código IN201703). Danny A. J. Gómez-Ramírez was supported by the Vienna Science and Technology Fund (WWTF) as part of the Vienna Research Group 12-004.

## References


[1] B. Tongbram, A. Mandal, S. Sengupta, S. Chakrabarti, Impact of vertical inter-QDs spacing correlation with the strain energy in a coupled bilayer quantum dot heterostructure, Journal of Alloys and Compounds 725 (2017) 984–997. doi:10.1016/j.jallcom.2017.07.215.

[2] C. A. Kessler, M. Reischle, R. Robach, E. Koroknay, M. Jetter, H. Schweizer, P. Michler, Optical investigations on single vertically coupled InP/GaInP quantum dot pairs, Phys. Status Solidi B 249 (2012) 747–751. doi:10.1002/pssb.201200004.

[3] E. Koroknay, W.-M. Schulz, D. Richter, U. Rengstl, M. Reischle, M. Bommer, C. A. Kessler, R. Robach, H. Schweizer, M. Jetter, P. Michler, Vertically stacked and laterally ordered InP and In(Ga)As quantum dots for quantum gate applications, Phys. Status Solidi B 249 (2012) 737–746. doi:10.1002/pssb.201100814.

[4] Y. I. Mazur, V. Lopes-Oliveira, L. D. de Souza, V. Lopez-Richard, M. D. Teodoro, V. G. Dorogan, M. Benamara, J. Wu, G. G. Tarasov, E. M. Jr., Z. M. Wang, G. E. Marques, G. J. Salamo, Carrier transfer in vertically stacked quantum ring-quantum dot chains, Journal of Applied Physics 117 (2015) 154307. doi:http://dx.doi.org/10.1063/1.4918544.

[5] M. Elborg, T. Noda, T. Mano, T. Kuroda, Y. Yao, Y. Sakuma, K. Sakoda, Self-assembly of vertically aligned quantum ring-dot structure by multiple droplet epitaxy, Journal of Crystal Growth 477 (2017) 239–242. doi:https://doi.org/10.1016/j.jcrysgro.2017.03.023.

[6] C. Heyn, A. Küster, A. Gräfenstein, A. Ungeheuer, A. Graf, W. Hansen, Gaas quantum dot molecules filled into droplet etched nanoholes, Journal of Crystal Growth 477 (2017) 235–238. doi:http://dx.doi.org/10.1016/j.jcrysgro.2017.03.029.

[7] R. J. Warburton, Single spins in self-assembled quantum dots, Nature Materials 12 (2013) 483–493. doi:10.1038/NMAT3585.

[8] M. Schorlemmer, A. Smaill, K.-U. Kühnberger, O. Kutz, S. Colton, E. Cambouropoulos, A. Pease, Coinvent: Towards a computational concept invention theory, in: 5th International Conference on Computational Creativity (ICCC), Vol. 2014, 2014.

[9] F. Bou, J. Corneli, D. Gomez-Ramirez, E. Maclean, A. Peace, M. Schorlemmer, A. Smaill, The role of blending in mathematical invention, Proceedings of the Sixth International Conference on Computational Creativity (ICCC). S. Colton et. al., eds. Park City, Utah, June 29-July 2, 2015. Publisher: Brigham Young University, Provo, Utah. (2015) 55–62.

[10] M. Martinez, A. M. H. Abdel-Fattah, U. Krumnack, D. Gómez-Ramírez, A. Smaill, T. R. Besold, A. Pease, M. Schmidt, M. Guhe, K.-U. Kühnberger, Theory blending: extended algorithmic aspects and examples, Annals of Mathematics and Artificial Intelligence (2016) 1–25doi:10.1007/s10472-016-9505-y.
URL http://dx.doi.org/10.1007/s10472-016-9505-y

[11] R. Manjarres-García, G. E. Escorcia-Salas, J. Manjarres-Torres, I. D. Mikhailov, , J. Sierra-Ortega, Double-donor complex in vertically coupled quantum dots in a threading magnetic field, Nanoscale Research Letters 7 (2012) 1. doi:https://doi.org/10.1186/1556-276X-7-531.

[12] L.-X. Zhai, Y. Wang, Z. An, Excitons and trions in single and vertically coupled quantum dots under an electric field, Physics Letters A 381 (2017) 2412–2419. doi:https://doi.org/10.1016/j.physleta.2017.05.017.

[13] V. Stavrou, Light effects in asymmetric vertically coupled InAs/GaAs quantum dots, Physica B 479 (2015) 6–9. doi:http://dx.doi.org/10.1016/j.physb.2015.09.024.

[14] Y. Li, Magnetization and magnetic susceptibility in nanoscale vertically coupled semiconductor quantum rings, Journal of Computational Electronics 4 (2005) 135–138. doi:https://doi.org/10.1007/s10825-005-7124-7.

[15] C. B. J. Fernández P, L. Jaimes Osorio, Energy levels of on-axis donors in vertically stacked quantum dots with different morphologies, Microelectronics Journal 39 (2008) 1259–1260. doi:10.1016/j.mejo.2008.01.008.

[16] F. G. I. D. Mikhailov, J. H. Marín, Off-axis donors in quasi-two-dimensional quantum dots with cylindrical symmetry, Phys. Status Solidi (b) 242 (2005) 1636–1649. doi:10.1002/pssb.200540053.

[17] M. R. Fulla, F. Rodriguez-Prada, J. H. M. Cadavid, Spectral properties of two electrons vertically coupled in toroidal quantum rings, Superlattices and Microstructures 49 (2011) 252–257. doi:https://doi.org/10.1016/j.spmi.2010.07.002.

[18] G. H. Li, A. R. Goñi, K. Syassen, O. Brandt, K. Ploog, State mixing in InAs/GaAs quantum dots at the pressure-induced $\Gamma - X$ crossing, Phys. Rev. B 50 (1994) 18420–18425. doi:https://doi.org/10.1103/PhysRevB.50.18420.

[19] E. Reyes-Gómez, N. Raigoza, L. E. Oliveira, Effects of hydrostatic pressure and aluminum concentration on the conduction-electron $g$ factor in GaAs-(Ga,Al)As quantum wells under in-plane magnetic fields, Physical Review B 77 (2008) 115–308. doi:10.1103/PhysRevB.77.115308.

[20] E. Kasapoglu, The hydrostatic pressure and temperature effects on donor impurities in $GaAs/Ga_{1x}Al_xAs$ double quantum well under the external fields, Physics Letters A 373 (2008) 140–143. doi:10.1016/j.physleta.2008.10.080.

[21] F. J. Culchac, N. Porras-Montenegro, A. Latgé, Hydrostatic pressure effects on electron states in GaAs(Ga, Al)As double quantum rings, Journal of

Applied Physics 105 (9) (2009) 094324. doi:10.1063/1.3124643.
URL https://doi.org/10.1063/1.3124643

[22] A. Lorke, R. J. Luyken, A. O. Govorov, J. P. Kotthaus, J. M. Garcia, P. M. Petroff, Spectroscopy of nanoscopic semiconductor rings, Physical Review Letters 84 (2000) 2223.

[23] V. M. Fomin, Physics of Quantum Rings, Springer-Verlag, Germany, 2014.

[24] M. R-Fulla, J. Marín, Y. A. Suaza, C. Duque, M. E. Mora-Ramos, States of an on-axis two-hydrogenic-impurity complex in concentric double quantum rings, Physics Letters A 378 (2014) 2297–2302.

[25] J. Castrillón, M. Fulla, J. Marín, D. Fonnegra-García, Y. Suaza, J. Salazar-Santa, Analysis of the eigenstates of a semiconductor hydrogenic washer-shaped structurally deformed nanoring: External crossed fields and stark-like effects, Physica B: Condensed Matter 521 (2017) 17–27. doi:https://doi.org/10.1016/j.physb.2017.06.036.

[26] J.-L. Zhu, Z. Dai, Two electrons in one-dimensional nanorings: Exact solutions and interaction energies, Phys. Rev. B 68 (2003) 045324. doi:10.1103/PhysRevB.68.045324.